Vietnam Journal of Science and Technology ***64****(1) (2026) 68–77*
DOI: https://doi.org/10.15625/2525-2518/18599

Influence of coating time on characterization of hydroxyapatite (HAp) coating on WE43 alloy by a chemical solution deposition method

Anh Tuyet Thi Ngo[1,2,*], Sachiko Hiromoto[2], Linh Do Chi[1], Hanh Hong Pham[1], San Thy Pham[1], Hoa Bui Thi[1], Thai Hong Giang[1]

[1]*Institute of Materials Science, Vietnam Academy of Science and Technology, 18 Hoang Quoc Viet Road, Nghia Do Vard, Ha Noi, Viet Nam*
[2]*Research Center for Structural Materials, National Institute for Materials Science, 1-2-1 Sengen, Tsukuba 305-0047, Japan*

[*]Email: *anhtuyet20379@gmail.com*

Received: 01 August 2023; Accepted for publication: 10 October 2023

Abstract. In this study, hydroxyapatite layers (HAp) were formed on a Mg-4 % Y-3 % rare earth alloy (WE43) by a chemical solution deposition method at various coating times, from 0.5 hours to 4 hours. The adhesion of the HAp layers was evaluated by the pull-off test method. The corrosion resistance of these coatings was measured by polarization tests and Nyquist impedance spectrum performed in a simulated body fluid (SBF) at 37±1 °C. XRD analysis demonstrated that HAp coating layers were formed in the whole specimens, while the highest intensity of the HAp peak was recorded for specimens with coating times of 2 and 4 hours. Adhesion test results showed that the HAp layer coated for 2 hours had the highest adhesion strength of 6.46 MPa, which is due to the very dense structure and rod-shaped HAp crystals of the outer-coating layer. The corrosion and formation of $Mg(OH)_2$ under the HAp layers were responsible for the decrease in adhesion strength. Polarization tests in SBF at 37±1 °C showed that the corrosion current density decreased with coating time from 0.5 to 2 hours, and the HAp layer on WE43 was formed on the specimen with a coating time of 2 hours, resulting in significantly improved corrosion resistance compared to other coating times.

Keywords: HAp coating, coating time, adhesion strength, corrosion, biodegradable.

Classification numbers: 3.4, 3.5.

1. INTRODUCTION

Classic metallic biomaterials such as pure titanium and its alloys, CoCr alloys, and stainless steel have been employed extensively in bone replacement and bone fixation devices in recent years to repair bone fractures or promote healing. However, these types of traditional metallic biomaterials required secondary surgery in order to remove the implants after healing [1, 2]. Bioabsorbable implants have emerged as an alternative to avoid long-term complications caused by permanent implants in applications that require a device with a temporary short function, such as endovascular stents and bone repair implants [3]. Mg and some of its alloys are biocompatible and have good mechanical properties, which make them good candidates for biodegradable

applications [3]. The density and elastic modulus of Mg alloys are 1.74–2.0 g/cm^3 and 41–45 GPa, respectively, which are well matched with those of human bone. Mg is non-toxic to the human body and is degradable in the body fluid. Magnesium alloys are potential options for biodegradable materials because of the benefits listed above [4-6]. Additionally, the Young's modulus of Mg alloys is similar to that of bone, avoiding stress shielding effect, which occurs for metallic implant materials with high Young's modulus [2, 4]. In the human body, the bioabsorbable magnesium devices should keep their original strength until the affected part of the body has healed [5, 6]. Magnesium is the fourth plenteous element in the body and is necessary for physiological functions. The byproducts of magnesium in the human body are non-toxic, and the excess amount of magnesium will be excreted through natural metabolism [7, 8]. Despite all the advantages, Mg and its alloys rapidly corrode in the physiological environment, with a pH value in the range of 7.2–7.4, which results in a loss of mechanical strength and causes the implants to fail early [9]. The corrosion process also produces hydrogen (H_2) gas around the implants [10-14]. This leads to the limitations in Mg applications, and commercial implants are still unavailable [9]. Therefore, the corrosion process must be slowed down for implant applications. It is essential to control the degradation rate of Mg alloys for practical applications in medicine. Among many biodegradable Mg alloy series, Mg-rare earth (Mg-RE) alloys are only ones which have been used for clinical trials [15]. Numerous investigations have shown that both the properties and functional activity of any implantable biomaterial can be influenced by surface modifications, such as polishing, oxidation, passivation, coating deposition, ion-implantation, etc. Of these techniques, the application of synthetic calcium orthophosphate coatings appears to be the most effective way of achieving surface modification, and moreover improves the biocompatibility and osteointegration of metallic implants [16]. The results suggested that HAp coated WE43 showed the highest corrosion resistance compared with that of all other materials [15, 17]. Kim *et al.* [18] applied solution treatment method to form a HAp layer on the surface of Mg substrate. The research demonstrated that the HAp coating layer significantly improved the corrosion resistance and biological response including cell attachment, proliferation and differentiation of osteoblasts [4]. Rahman *et al*. coated dicalcium phosphate dihydrate ($CaHPO_4.2H_2O$, DCPD) and HAp on the surface of WE43 magnesium alloy and pure Mg by chemical solution treatment method. According to the results, WE43 coated with HAp possessed superior corrosion resistance compared with all other tested materials [13]. Our recent research also demonstrated that HAp-WE43 has a slow degradation rate, making it suitable for temporary implant applications [15, 19].

In this paper, the effect of coating time on the structure, composition, corrosion resistance and adhesion of hydroxyapaitite coatings on WE43 material by the chemical solution method is investigated. The adhesion of HAp layers was measured by the pull-off method. The effect of coating time on the mophological structure of HAp layers was examined by the SEM method. The corrosion resistance of HAp coatings is also evaluated by a polarization test and Nyquist impedance spectrum.

2. MATERIALS AND METHODS

2.1. Material preparation

Extruded WE43 magnesium alloy (Y 4.0 mass%, Nd 2.3 mass%, RE 1.1 mass%, Zr 0.48 mass%, Zn+Ag 0.03 mass%, Cu 0.002 mass%, Mg 0.01 mass%, Fe 0.001 mass%, Li 0.1 mass%, Ni 0.000 mass%, Mg Bal.) supplied by Osaka Fuji Industrial Co., Ltd. was used as a substrate. The cylindrical alloy rod, 16.7 mm in diameter, was sectioned into disc-shaped samples

with a thickness of 2 mm. The samples were then polished using SiC papers with grit sizes ranging from #400 to #1200. Prior to the coating process, the sample surfaces were cleaned with ethanol and dried. The coating solution in this investigation was formulated with ethylenediaminetetraacetic acid calcium disodium salt hydrate ($C_{10}H_{12}N_2O_8Na_2Ca$), potassium dihydrogen phosphate (KH_2PO_4), and sodium hydroxide (NaOH). Equal volumes of 0.5 mol/L Ca-EDTA and 0.5 mol/L KH_2PO_4 were combined, and NaOH solution was subsequently added to adjust the pH of the coating solution to 8.6. The solution was heated to 90 °C. The samples were immersed in the treatment solutions at 90ºC and a range of coating time from 0.5 hours to 4 hours. After the coating process, the samples were taken out, washed with deionized water, and allowed to air-dry at room temperature prior to analyzed properties of the samples. The samples coated at coating time of 0.5, 1, 2 and 4hours were named t-0.5h, t-1h, t-2h and t-4h-samples, respectively.

2.2. Material characterization

The crystal structure of the coated samples was analyzed using X-ray diffractometry (XRD; Bruker, D2 Phaser). The surface and cross-sectional morphologies were examined with a backscattered electron microscope (SEM; HITACHI, Miniscope TM-1000) and a field-emission scanning electron microscope (FE-SEM; FEI, Quanta FEG250) equipped with an energy-dispersive X-ray spectrometer (EDS; TEAM EDS, EDAX).

2.3 Electrochemical measurements

The polarization test and Nyquist impedance spectrum were carried out for the t-0.5h, t-1h, t-2h and t-4h specimens in SBF with its chemical composition such as: 8.00 g/L of NaCl; 0.40 g/L of KCl; 0.18g/L of $CaCl_2$; 0.35 g/L of $NaHCO_3$; 0.48 g/L of $Na_2HPO_4{\cdot}2H_2O$; 0.10 g/L of $MgCl_2{\cdot}6H_2O$; 0.06 g/L of KH_2PO_4; 0.10 g/L of $MgSO_4{\cdot}7H_2O$; 1.00 g/L of glucose at 37 ± 1 °C by a potentiostat (Autolab PGSTAT-302N, Metrohm/Netherlands). The samples were prepared to fit a 16.7 mm diameter holder electrode. A three-electrode setup was employed, with the specimen as the working electrode, platinum as the counter electrode, and saturated Ag/AgCl as the reference electrode. The open circuit potential (OCP) was monitored for 600 s. In addition, the Nyquist impedance spectra were recorded at the open circuit potential (OCP) over a frequency range of 100,000 Hz to 0.01 Hz with an amplitude of 10 mV. Polarization curves were obtained within a potential of −0.25 V to +0.5 V versus OCP at a scan rate of 1 mV/s.

2.4. Adhesion test

In this investigation, the adhesion strength of the HAp coating was evaluated using a pull-off method with PosiTest® AT pull-off adhesion testers (Quick Guide V.5.2), following the ASTM D4541-17 standard. An Al dolly with a diameter of 10 mm was glued onto the surface of the coating using an epoxy resin (Epoxy Adhesives Araldite® 2011-A/B). A preload of 2 N was applied to the dolly for 24 h at room temperature. The dolly was then pulled off at a crosshead rate of 4.0 MPa/s until complete detachment from the specimen. Each adhesion test was performed in triplicate. The adhesion strengths were calculated as the average of three measurements for each pH of the coating solution, and error bars were generated using Excel 2016.

3. RESULTS AND DISCUSSION

3.1. Formation of coating layers on WE43 substrate

Figure 1 shows the XRD patterns of HAp coated WE alloy treated in coating solutions at pH 8.6 with coating times ranging from 0.5 to 4 hours. There are some diffraction peaks originating from HAp at all coating times indicating that HAp layers had formed on the WE43 alloy. However, for the t-0.5h and t-1h specimens, the intensity of the HAp peaks is weak at 2Θ of 26.7 (002)-HAp and the Mg-substrate peaks were observed. For the t-2h and t-4h specimens, the peaks of HAp appeared with strong intensity of (002)-HAp and some weak intensity HAp peaks of (102), (213) and (004)-HAp. Simultaneously, small and broad peaks of $Mg(OH)_2$ appeared due to the corrosion of the Mg-substrate during the coating process.

The surface morphology of the t-0.5h specimen is illustrated in Figure 2a, showing a hillside-like structure and small rod-shaped crystals. The surface morphology of the t-1h specimen showed a rod-shaped crystal structure with larger dimensions. Meanwhile, as the coating time increased to 2-4 h, a flower-like structure appeared on the surface, with greater density and uniformity. According to the cross-sectional morphology in Figures 2b-2n, the coatings of all the specimens had a two-layer structure including an inner solid layer and an outer porous layer.

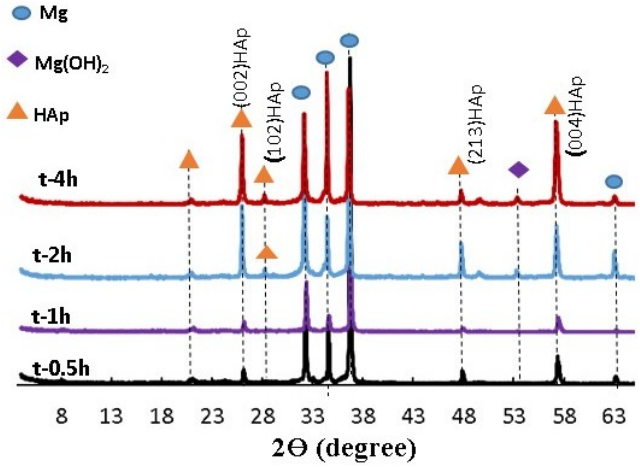

Figure 1. XRD patterns of t-0.5h, t-1h, t-2h and t-4h specimens.

Figure 2 shows surface and cross-sectional SEM images of t-0.5h, t-1h, t-2h and t-4h specimens. The HAp layer of the t-0.5h specimen was composed of an outer sparse layer with very thin rod-shaped crystals and an inner solid layer. At the boundary between the substrate and HAp layers was a relatively dark wavy region, indicating that the substrate was corroded during the coating process, that should be a $Mg(OH)_2$ intermediate layer as previously reported [20, 21]. The thickness of the inner layers of the t-0.5h specimen was approximately 2 μm. The thickness of the layers increased with coating time. As a result, both the dense inner layer and the rod-like outer layer contributed significantly to the thickness of the coatings. The coatings' maximum thickness was attained with the t-4h specimen, approximately 5 μm. In parallel, the thickness of the $Mg(OH)_2$ intermediate layer increased dramatically with coating time, as observed in Figures 2(f), 2(k) and 2(n). The cracks and pores in the inner layers in Figures 2(k) and 2(n) were most likely formed during cross-sectioning and grinding. These nanopores and cracking suggested that the inner layers were relatively fragile.

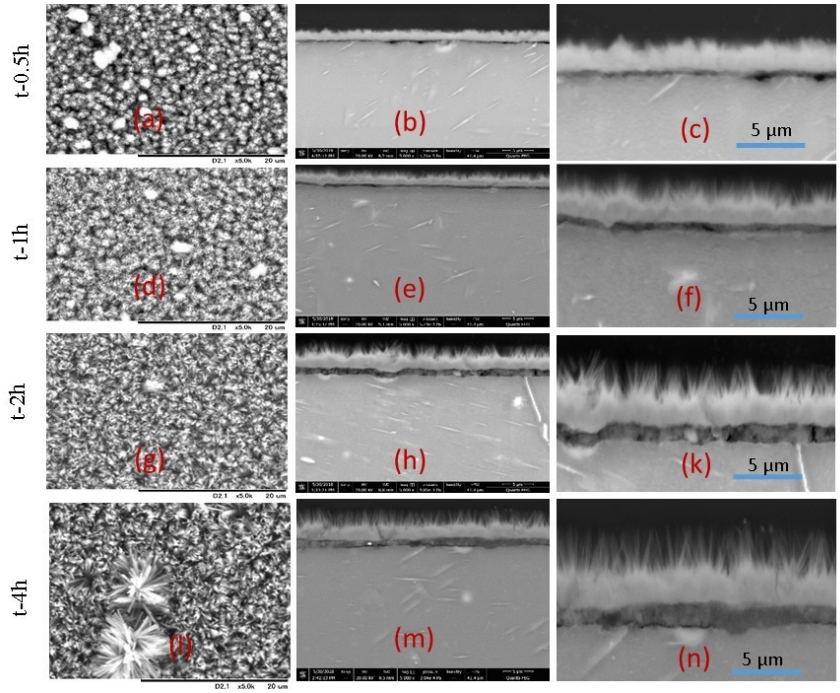

Figure 2. Surface and cross-sectional morphology of HAp coating on WE43: (a) surface morphology; (b)-(c) cross-sectional morphology of t-0.5h specimen; (d) surface morphology; (e)-(f) cross-sectional morphology of t-1h specimen; (g) surface morphology; (h)-(k) cross-sectional morphology of t-2h specimen; (l) surface morphology; (m)-(n) cross-sectional morphology of t-4h specimen.

The mechanism of HAp coating formation is shown in Figure 3 and includes 3 stages:

Firstly, when the WE43 substrate is immersed in the solution prepared as in Section 2.1, the corrosion reaction of the Mg alloys occurs as described by Eqs. (1) and (2):

$$Mg \rightarrow Mg^{2+} + 2e \quad (1)$$

$$2H_2O + 2e \rightarrow 2OH^- + H_2 \quad (2)$$

H_2 gas is generated and the pH of the surrounding environment increases. The generation of OH^- groups from Eq. (2) increases the pH on the surface, leading to the simultaneous acceleration of the formation of HA nuclei and $Mg(OH)_2$ according to the reactions described by Eqs. (3) and (4):

$$Mg^{2+} + 2OH^- \rightarrow Mg(OH)_2 \quad (3)$$

$$10Ca^{2+} + 6PO_4^{3-} + 2OH^- \rightarrow Ca_{10}(PO_4)_6(OH)_2 \quad (4)$$

Secondly, as the coating time increases, the HAp nuclei grow and transform into HAp crystals, resulting in the formation of a denser inner HAp layer.

Finally, the HAp crystals grow larger and form rods in the outer HAp layer.

According to this mechanism, after a brief coating time, HAp nuclei are formed on the surface, and then these nuclei gradually develop into “hillside” patterns. As the coating time increases, the HAp crystals grow larger and form rods as observed in Figure 3, leading to an

increase in the thickness of the coating. These results are consistent with previous studies [20, 22].

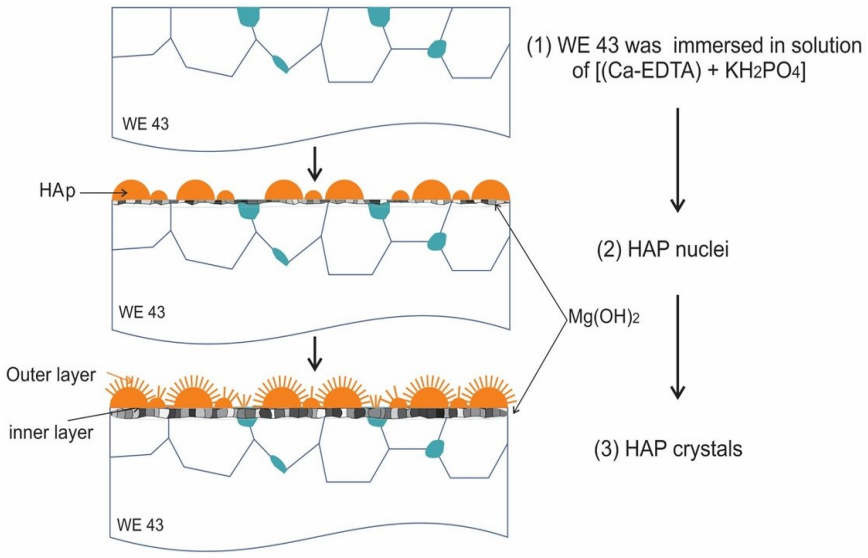

Figure 3. Mechanism of HAp coating formation on WE43 substrate.

3.2. Corrosion behavior of HAp-coated WE43 alloy

3.2.1. Polarization behavior

Figure 4 shows the polarization curves of the t-0.5h, t-1h, t-2h, and t-4h specimens in SBF at 37 °C. The corrosion potential (E_{corr}) and corrosion current density (i_{corr}) were determined by a Tafel extrapolation method using NOVA software version 1.10 and the corrosion rates (RM) were calculated from the polarization curves. The electrochemical parameters are shown in Table 1.

Table 1. Electrochemical parameters.

No	Specimen	E_{corr} (V)	i_{corr} (μA/cm^2)	CR (mm/year)
1	t-0.5h	-1.495	11.355	0.512
2	t-1h	-1.420	8.972	0.405
3	t-2h	-1.351	4.947	0.223
4	t-4h	-1.538	14.313	0.646

The i_{corr} value of the t-0.5h specimen was 11.355 μA/cm^2. The i_{corr} values of the coated samples at various coating time were 8.972, 4.947, and 14.313 μA/cm^2 for the t-1h, t-2h, and t-4h specimens, respectively. The results showed that with 2 hours of coating, the i_{corr} value of the sample reached its lowest level at 4.947 μA/cm^2. The corrosion potential (E_{corr}) value of the t-0,5h specimen was -1.495 V while the E_{corr} values of the t-1h, t-2h, and t-4h specimens were -1.420, -1.351, and -1.538 V, respectively. The E_{corr} value shifts in the positive direction as the coating treatment time in the solution increases up to 2 hours. Additionally, the corrosion rate values of the specimens are in agreement with the i_{corr} and E_{corr} values. These results confirmed that the corrosion resistance of the coated specimens increased with the coating treatment time, up to 2 hours, due to the higher thickness of the dense structure of the inner HAp layer, which improves the corrosion protectiveness for the specimens. However, at the coating time of 4 hours,

the coated specimens' corrosion resistance started to decline. Although the coating of the t-4h specimen was thicker than that of the t-2h specimen, its corrosion resistance was lower. It could be explained by the formation of an intermediate $Mg(OH)_2$ layer with a nanoporous structure at a coating time of 4 hours, which had a higher thickness compared to the t-2h specimen.

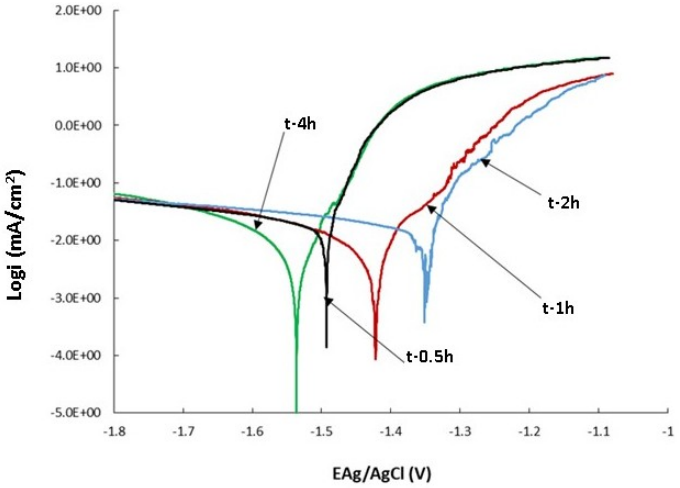

Figure 4. Polarization curves of HAp-coated WE43 alloy specimens in SBF.

3.2.2. Nyquist impedance spectrum

In order to gain a better insight into the Mg alloy corrosion process, electrochemical impedance spectroscopy (EIS) was used to investigate the electrode corrosion resistance and to obtain information about the processes occurring at the electrode/electrolyte interface before and after electrolyte renewal.

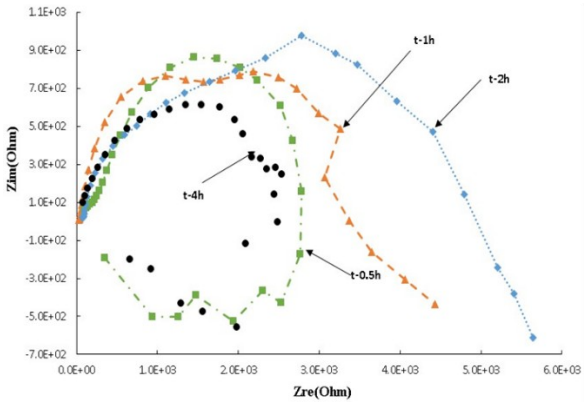

Figure 5. Nyquist impedance spectrum of HAp-coated WE43 alloy specimens in SBF.

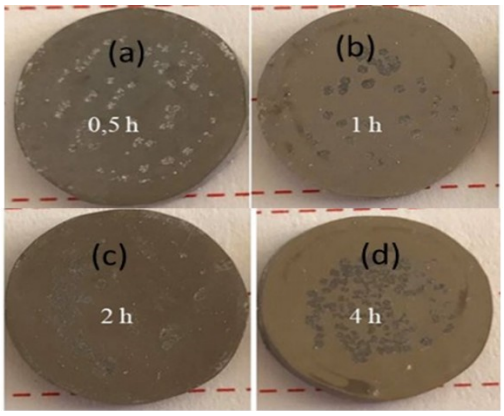

Figure 6. Surface images of (a) t-0.5h, (b) t-1h, (c) t-2h, and (d) t-4h specimens after polarization tests in SBF.

Figure 5 shows Nyquist impedance spectrum of the specimens. The overall increase in Zre values of the specimens can be related to the formation of an inner $Mg(OH)_2$ passive layer and an HAp coating with increasing coverage over the coating time up to 2 hours. The smaller Zre values of the t-4h specimen observed can be related to the occurrence of a localized corrosion process,

creating surface pitting, with a reduced diffusion resistance due to the nanoporous structure of the $Mg(OH)_2$ layer. The t-2h specimen has the highest Zre value, reaching approximately 6000 Ohms. Thus, the t-2h specimen has the best corrosion resistance. Figure 6 shows images of the HAp-coated WE43 alloy after polarization tests. The surfaces showed corrosion pits on the entire surface. The number of pits of the t-4h specimen was the largest, which was consistent with the high corrosion current density as indicated in Table 1. The number of pits on the t-1h and t-2h specimens was fewer than that of the t-0.5h and t-4h specimens, indicating that the HAp coatings with a coating time of 1 to 2 hours provide better protectiveness compared to other coating times.

3.3. Adhesion strength of HAp coatings

Generally, adhesion strength of HAp-coated WE43 alloy specimens increased with the coating time. However, when increasing the coating time to 4 hours, the adhesion decreased. As the samples were soaked for too long time in the coating solution, besides the nucleation and growth of HAp nuclei to form the HAp coating, there is also a corrosion reaction of magnesium, causing cracking in the dense layer under the WE43 substrate [4, 15]. The corrosion and formation of $Mg(OH)_2$ under the HAp layers were responsible for the decrease in adhesion strength. Figure 8 shows the surface SEM images the t-0.5h, t-1h, t-2h and t-4h specimens before and after the adhesion test. The surface SEM images of dollies after the adhesion test are also shown in Figure 8. Before the adhesion test, the surfaces of the specimens exhibited the leaf-shaped and rod-shaped structures characteristic of the HAp coating (Figure 2) as mentioned in Section 3.1 of this investigation. After the adhesion test, no HAp layer was observed on the specimen surface. In other words, during the adhesion measurement test the whole HAp coating was pulled off from the WE43 substrate.

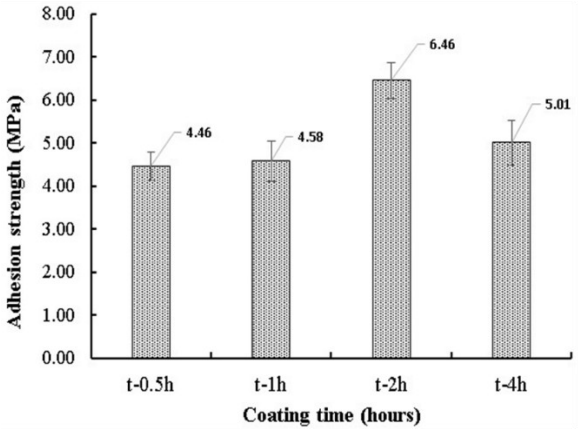

Figure 7. Adhesion strength of HAp-coated WE43 alloy specimens

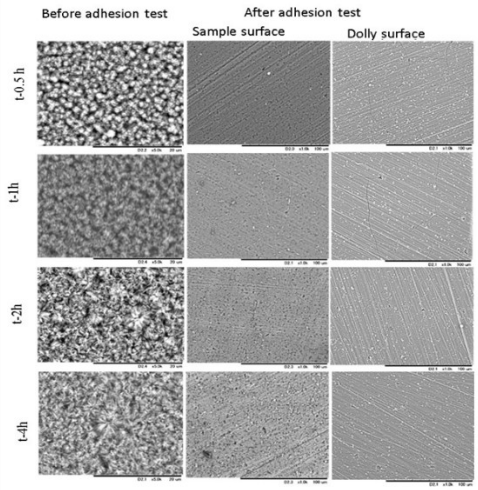

Figure 8. Surface SEM images of t-0.5h, t-1h, t-2h, and t-4h specimens.

4. CONCLUSIONS

WE43 magnesium alloy was treated in a coating solution, containing ethylenediaminetetraacetic acid calcium disodium salt hydrate (Ca-EDTA: $C_{10}H_{12}N_2O_8Na_2Ca$), potassium dihydrogen phosphate (KH_2PO_4) and sodium hydroxide (NaOH), at pH 8.6 for 0.5 to

4 hours. The HAp coatings of WE43 consisted of an inner dense layer and an outer coarse layer. The inner dense layer of WE43 was composed of densely packed, dome-shaped precipitates with various sizes, and the outer layer consisted of rod-like crystals growing from each dome in a radial direction. The thickness of the coating increased with the coating time and the structure also changed from densely rough for the t-0.5h specimen to leaf-shaped and rod-shaped for the t-2h and t-4h specimens. The highest adhesion was achieved at approximately 6.46 MPa and the best corrosion resistance was demonstrated for the t-2h specimen.

Acknowledgments. This work was funded by the Vietnam Academy of Science and Technology (VAST) under grant number VAST03.02/22-23.

CRediT authorship contribution statement. Anh Tuyet Thi Ngo: Conceptualization, Investigation, Formal analysis,Writing – original draft. Sachiko Hiromoto: Investigation, Formal analysis, Writing – original draft. San Thy Pham: Validation, Writing – review & editing. Linh Do Chi, Hanh Hong Pham, Hoa Bui Thi, Thai Hong Giang: Writing – review & editing.

Declaration of conflicting interests. The authors declared no potential conflicts of interest with respect to the research, authorship, and/or publication of this article.

REFERENCES

1. Cao N. Q., Pham D. N., Kai N., Dinh H. V., Hiromoto S., Kobayashi E. - In vitro corrosion properties of mg matrix in situ composites fabricated by spark plasma sintering. Metals, **7**(9) (2017) 358. https://doi.org/10.3390/met7090358.
2. Chiu C., Lu C. T., Chen S. H., Ou K. L. - Effect of Hydroxyapatite on the Mechanical Properties and Corrosion Behavior of Mg-Zn-Y Alloy. Materials (Basel), **10**(8) (2017) 855. https://doi.org/10.3390/ma10080855.
3. Ascencio M., Pekguleryuz M., Omanovic S. - An investigation of the corrosion mechanisms of WE43 Mg alloy in a modified simulated body fluid solution: The effect of electrolyte renewal. Corros. Sci., **91** (2015) 297-310. https://doi.org/10.1016/j.corsci.2014.11.034.
4. Ngo T. T. A., Hiromoto S., Pham S. T., Cao N. Q. - Adhesion properties of hydroxyapatite and octacalcium phosphate coating layers to AZ31 alloy formed at various pH values. Surf. Coat. Technol., **381** (2020) 125187. https://doi.org/10.1016/j.surfcoat.2019.125187.
5. Hiromoto S., Shishido T., Yamamoto A., Maruyama N., Somekawa H., Mukai T. - Precipitation control of calcium phosphate on pure magnesium by anodization. Corros. Sci., **50**(10) (2008) 2906-2913. https://doi.org/10.1016/j.corsci.2008.08.013.
6. Hiromoto S., Yamamoto A. - Control of degradation rate of bioabsorbable magnesium by anodization and steam treatment. Mater. Sci. Eng. C, **30**(8) (2010) 1085-1093. https://doi.org/10.1016/j.msec.2010.06.001.
7. Rahimi M., Mehdinavaz Aghdam R., Sohi M. H., Rezayan A. H., Ettelaei M. - Improving biocompatibility and corrosion resistance of anodized AZ31 Mg alloy by electrospun chitosan/mineralized bone allograft (MBA) nanocoatings. Surf. Coat. Technol., **405** (2021) 126627. https://doi.org/10.1016/j.surfcoat.2020.126627.
8. Suchanek K., Perzanowski M., Suchy K., Lekka M., Szaraniec B., Marszałek M. - Assessment of phase stability and in vitro biological properties of hydroxyapatite coatings composed of hexagonal rods. Surf. Coat. Technol., **364** (2019) 298-305. https://doi.org/10.1016/j.surfcoat.2019.02.088.
9. Tuyet T. A. N., Hiromoto S., Nguyen P. N., San T. P. - Effect of pH of coating solution on adhesion strength of hydroxyapatite and octacalcium phosphate coatings on AZ31 magnesium

alloy. Mater. Sci. Forum, **985** (2020) 156-164. https://doi.org/10.4028/www.scientific.net/msf.985.156.

10. Li L.-H., Narayanan T. S. N., Kim Y. K., Kong Y.-M., Shin G.-S., Lyu S.-K., Park I. S., Lee M. H. - Coloring and corrosion resistance of pure Mg modified by micro-arc oxidation method. Int. J. Precis. Eng. Manuf., **15**(8) (2014) 1625-1630. https://doi.org/10.1007/s12541-014-0512-9.
11. Liu L., Koo Y., Collins B., Xu Z., Sankar J., Yun Y. - Biodegradability and platelets adhesion assessment of magnesium-based alloys using a microfluidic system. PLoS One, **12**(8) (2017) e0182914. https://doi.org/10.1371/journal.pone.0182914.
12. Salman S. A., Kuroda K., Okido M. - Preparation and characterization of hydroxyapatite coating on AZ31 mg alloy for implant applications. Bioinorg. Chem. Appl., **2013** (2013) 175756. https://doi.org/10.1155/2013/175756.
13. Rahman M., Li Y., Wen C. - HA coating on Mg alloys for biomedical applications: A review. J. Magnes. Alloys, **8**(3) (2020) 929-943. https://doi.org/10.1016/j.jma.2020.05.003.
14. Mousa H. M., Chan H. P., Kim C. S. - Surface modification of magnesium and its alloys using anodization for orthopedic implant application. In *Magnesium Alloys*, InTech (2017).
15. Ngo T. T. A., Hiromoto S., Do L. C., Pham H. H., Hanh L. - Effect of pH of coating solution on the adhesion strength and corrosion resistance of hydroxyapatite and octacalcium phosphate coated WE43 alloy. J. Biomater. Appl., **36**(3) (2021) 428-440. https://doi.org/10.1177/08853282211012525.
16. Dorozhkin S. V. - Calcium orthophosphate coatings on magnesium and its biodegradable alloys. Acta Biomater., **10**(7) (2014) 2919-2934. https://doi.org/10.1016/j.actbio.2014.02.026.
17. Byun S. H., Lim H. K., Cheon K. H., Lee S. M., Kim H. E., Lee J. H. - Biodegradable magnesium alloy (WE43) in bone-fixation plate and screw. J. Biomed. Mater. Res. B Appl. Biomater., **108**(6) (2020) 2505-2512. https://doi.org/10.1002/jbm.b.34582.
18. Kim S. M., Jo J. H., Lee S. M., Kang M. H., Kim H. E., Estrin Y., Lee J. H., Lee J. W., Koh Y. H. - Hydroxyapatite-coated magnesium implants with improved *in vitro* and *in vivo* biocorrosion, biocompatibility, and bone response. J. Biomed. Mater. Res. A, **102**(2) (2014) 429-441. https://doi.org/10.1002/jbm.a.34718.
19. Hiromoto S., Itoh S., Noda N., Yamazaki T., Katayama H., Akashi T. - Osteoclast and osteoblast responsive carbonate apatite coatings for biodegradable magnesium alloys. Sci. Technol. Adv. Mater., **21**(1) (2020) 346-358. https://doi.org/10.1080/14686996.2020.1761237.
20. Tomozawa M., Hiromoto S. - Growth mechanism of hydroxyapatite-coatings formed on pure magnesium and corrosion behavior of the coated magnesium. Appl. Surf. Sci., **257**(19) (2011) 8253-8257. https://doi.org/10.1016/j.apsusc.2011.04.087.
21. Tomozawa M., Hiromoto S., Harada Y. - Microstructure of hydroxyapatite-coated magnesium prepared in aqueous solution. Surf. Coat. Technol., **204**(20) (2010) 3243-3247. https://doi.org/10.1016/j.surfcoat.2010.03.023.
22. Hiromoto S., Tomozawa M. - Hydroxyapatite coating of AZ31 magnesium alloy by a solution treatment and its corrosion behavior in NaCl solution. Surf. Coat. Technol., **205**(19) (2011) 4711-4719. https://doi.org/10.1016/j.surfcoat.2011.04.036.